623

Fermilab Library
0 1160 0038890 4

MIDWESTERN UNIVERSITIES RESEARCH ASSOCIATION

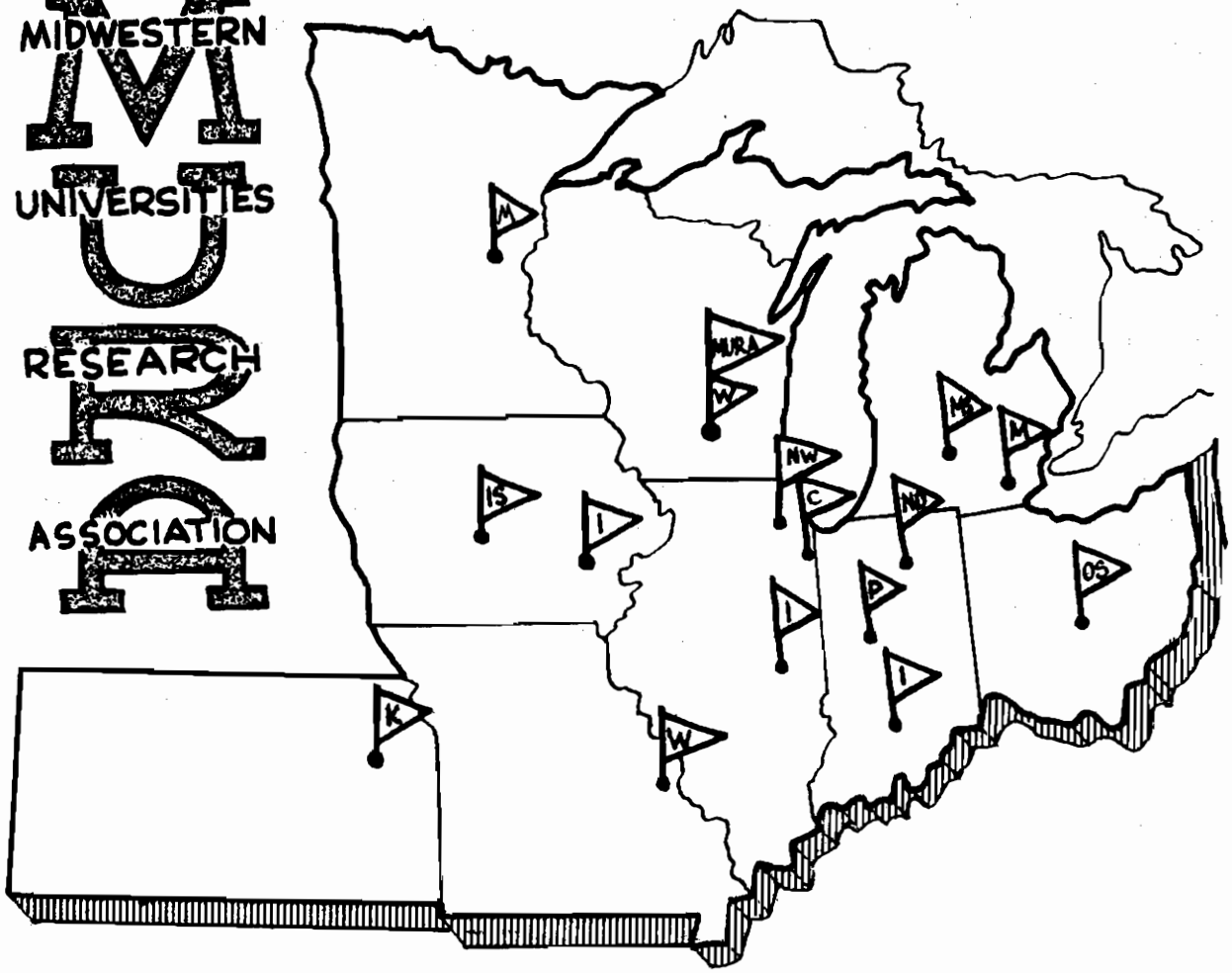

THE EFFECT OF CURVATURE ON THE FIELDS IN A CIRCULAR ACCELERATOR

J. Van Bladel

REPORT **NUMBER** 623

LEGAL NOTICE

This report was prepared as an account of Government sponsored work. Neither the United States, nor the Commission, nor any person acting on behalf of the Commission:

A. Makes any warranty or representation, expressed or implied, with respect to the accuracy, completeness, or usefulness of the information contained in this report, or that the use of any information, apparatus, method, or process disclosed in this report may not infringe privately owned rights; or

B. Assumes any liabilities with respect to the use of, or for damages resulting from the use of any information, apparatus, method, or process disclosed in this report.

As used in the above, "person acting on behalf of the Commission" includes any employee or contractor of the Commission, or employee of such contractor, to the extent that such employee or contractor of the Commission, or employee of such contractor prepares, disseminates, or provides access to, any information pursuant to his employment or contract with the Commission, or his employment with such contractor.

Printed in USA. Price $0.50. Available from the

Office of Technical Services
U. S. Department of Commerce
Washington 25, D. C.

MURA-623
UC-28, Particle Accelerators and
High Voltage Machines
TID-4500 (16th Edition)

MIDWESTERN UNIVERSITIES RESEARCH ASSOCIATION*

2203 University Avenue, Madison, Wisconsin

THE EFFECT OF CURVATURE ON THE FIELDS IN A CIRCULAR ACCELERATOR

J. Van Bladel

June 15, 1961

ABSTRACT

A comparison is made between the electromagnetic fields in a circular accelerator, and in the linear accelerator obtained by "developing" the circular structure. In both cases the fields are excited by a narrow gap perpendicular to the axis, and across which a constant radio-frequency voltage is applied.

*AEC Research and Development Report. Research supported by the U.S. Atomic Energy Commission, Contract No. AT(11-1)-384.

I. Introduction

Circular accelerators of the type shown in Figure 1 are often excited by a radio-frequency voltage applied across a narrow radial gap g. A typical method to generate this voltage consists of incorporating the gap into a surrounding resonant cavity, which is then excited at one of its resonant frequencies. The resonance phenomenon creates a large voltage across the gap. The resonant mode is commonly chosen to yield a practically constant voltage (in phase and amplitude) all along the gap contour. The tangential electric field in the gap will, in these circumstances, be described be the formula

$$\bar{E}_t = \frac{V}{r}\,\delta(\varphi)\,\bar{u}_\varphi \tag{1}$$

where $\bar{u}_\varphi$ is a unit vector in the direction of increasing azimuth φ. It is our purpose to calculate the fields inside the "doughnut" volume for such a field configuration. Furthermore, it is our intention to investigate the validity of the approximation in which the circular accelerator is replaced, locally at least, by a straight duct of identical cross-section. This simplification results in the replacement of the circular accelerator of Figure 1 by the rectangular wave-guide of Figure 2, excited by a periodic array of gaps. The spacing between gaps must be equal to the average length of a circular path. The field in the gap now becomes

$$\bar{E}_t = V\,\delta(y)\,\bar{u}_y \tag{2}$$

It is our goal to calculate the fields in the linear accelerator, and to compare them to those of the circular accelerator of similar cross-section. Our final purpose will be to get an idea of the error committed by neglecting the curvature of the vacuum chamber.

II. Fields in the Circular Accelerator

The accelerator of Figure 1 is nothing but a coaxial cavity with a given impressed tangential electric field across its boundary surface. The fields inside such a cavity can be calculated from a knowledge of the resonant modes, which can be written down explicitly for the coaxial geometry[1]. The relevant formulae can be found in the literature[2], and will not be reproduced here. Alternatively, the accelerator can be looked at as a coaxial wave-guide with given tangential electric field across its cylindrical wall and terminal flanges. Both approaches very naturally yield the same results. The second approach, which is perhaps less classical but more concise, is presented in some detail in the appendix. We only wish to quote the final results here. The formulae involve the following two kinds of basic functions:

---

1. See, for example, C.G. Montgomery "Technique of Microwave Measurements" Ch. 5 McGraw-Hill Book Co., 1947.

2. J.C. Slater: "Microwave Electronics" Ch. 4. Van Nostrand and Co., New York, 1950.

(a) Functions $R_m(\mu_{mp} r)$, linear combinations of Bessel and Neumann functions, vanishing at the inside and outside radii.

$$R_m(\mu_{mp} r) = J_m(\mu_{mp} r) + A_{mp} N_m(\mu_{mp} r)$$

where A_{mp} and μ_{mp} are determined by equations

$$\frac{J_m(\mu_{mp} b)}{N_m(\mu_{mp} b)} = \frac{J_m(\mu_{mp} a)}{N_m(\mu_{mp} a)} = -A_{mp} \qquad (3)$$

(b) Functions $S_m(\nu_{mp} r)$

$$S_m(\nu_{mp} r) = J_m(\nu_{mp} r) + B_{mp} N_m(\nu_{mp} r)$$

the first derivative of which vanish at the inside and outside radii.

$$\frac{J_m'(\nu_{mp} b)}{N_m'(\nu_{mp} b)} = \frac{J_m'(\nu_{mp} a)}{N_m'(\nu_{mp} a)} = -B_{mp} \qquad (4)$$

Tables of roots of (3) and (4) are very sketchy, and a program to compute the latter on an IBM 704 was written by Dr. J. McNall. With

In a similar manner, the magnetic field turns out to be:

$$H_r = j\omega\varepsilon V \sum_m \sum_p \left\{ \frac{m^2}{\pi \mu_{mp}^2 \gamma_{mp}} \cos m\varphi \frac{R_m}{r} \cdot \frac{\cosh \gamma_{mp} z - \cosh \gamma_{mp}(L-z)}{\sinh \gamma_{mp} L} \cdot \frac{\int_b^a \frac{R_m}{r} dr}{\int_b^a R_m^2 r\, dr} \right.$$

$$\left. + \frac{1}{\pi \nu_{mp}^2 \tau_{mp}} \cos m\varphi \frac{dS_m}{dr} \cdot \frac{\cosh \tau_{mp} z - \cosh \tau_{mp}(L-z)}{\sinh \tau_{mp} L} \cdot \frac{S_m(\nu_{mp} a) - S_m(\nu_{mp} b)}{\int_b^a S_m^2 r\, dr} \right\}$$

$$H_\varphi = -j\omega\varepsilon V \sum_m \sum_p \left\{ \frac{m}{\pi \mu_{mp}^2 \gamma_{mp}} \sin m\varphi \frac{dR_m}{dr} \frac{\cosh \gamma_{mp} z - \cosh \gamma_{mp}(L-z)}{\sinh \gamma_{mp} L} \cdot \frac{\int_b^a \frac{R_m}{r} dr}{\int_b^a R_m^2 r\, dr} \right.$$

$$\left. + \frac{m}{\pi \nu_{mp}^2 \tau_{mp}} \sin m\varphi \frac{S_m}{r} \cdot \frac{\cosh \tau_{mp} z - \cosh \tau_{mp}(L-z)}{\sinh \tau_{mp} L} \cdot \frac{S_m(\nu_{mp} a) - S_m(\nu_{mp} b)}{\int_b^a S_m^2 r\, dr} \right\}$$

$$H_z = -j\omega\varepsilon V \sum_m \sum_p \frac{1}{\pi \tau_{mp}^2} \cos m\varphi \cdot S_m \left[1 - \frac{\sinh \tau_{mp} z + \sinh \tau_{mp}(L-z)}{\sinh \tau_{mp} L} \right] \cdot \frac{S_m(\nu_{mp} a) - S_m(\nu_{mp} b)}{\int_b^a S_m^2 r\, dr}$$

(6)

III. Fields in the Linear Duct

Expressions for the fields inside the rectangular duct of Figure 2 are available for a structure with a single exciting gap[3]. The field of an array of gaps can be found by simple superposition of solutions. With the parameters indicated in Figure 2, where the y = 0 plane is half way between two gaps, one finds:

$$E_x = \frac{8V}{\pi d} \sum_{1,3} \sum_{1,3} \frac{(-1)^{\frac{m+n}{2}}}{n} \sin m\pi \frac{x}{d} \cos n\pi \frac{z}{L} \frac{\sinh S_{mn} \frac{\pi y}{d}}{\sinh S_{mn} \frac{\pi D}{2d}} \qquad -\frac{D}{2} < y < 0$$

$$E_y = -\frac{8Vd}{\pi^2} \sum_{1,3} \sum_{1,3} \frac{(-1)^{\frac{m+n}{2}} \gamma_{mn}^2}{mn\, S_{mn}} \cdot \cos m\pi \frac{x}{d} \cos n\pi \frac{z}{L} \frac{\cosh S_{mn} \frac{\pi y}{d}}{\sinh S_{mn} \frac{\pi D}{2d}}$$

$$E_z = -\frac{8V}{\pi L} \sum_{1,3} \sum_{1,3} \frac{(-1)^{\frac{m+n}{2}}}{m} \cos m\pi \frac{x}{d} \cdot \sin n\pi \frac{z}{L} \frac{\sinh S_{mn} \frac{\pi y}{d}}{\sinh S_{mn} \frac{\pi D}{2d}}$$

$$H_x = \frac{j\omega \varepsilon_0 8Vd}{\pi L} \sum_{1,3} \sum_{1,3} \frac{(-1)^{\frac{m+n}{2}}}{m\, S_{mn}} \cos m\pi \frac{x}{d} \sin n\pi \frac{z}{L} \frac{\cosh S_{mn} \frac{\pi y}{d}}{\sinh S_{mn} \frac{\pi D}{2d}}$$

$$H_z = \frac{j\omega \varepsilon_0 8V}{\pi} \sum_{1,3} \sum_{1,3} \frac{(-1)^{\frac{m+n}{2}}}{n\, S_{mn}} \sin m\pi \frac{x}{d} \cdot \cos n\pi \frac{z}{L} \frac{\cosh S_{mn} \frac{\pi y}{d}}{\sinh S_{mn} \frac{\pi D}{2d}}$$

(7)

3. J. Van Bladel "Fields in Gap-excited Rectangular Ducts" J. Appl. Phys. 23, 1479-1483, 1957.

where $S_{mn} = d\sqrt{\frac{m^2\pi^2}{d^2} + \frac{n^2\pi^2}{L^2} - k^2}$ $\qquad \gamma_{mn}^2 = \frac{m^2\pi^2}{a^2} + \frac{n^2\pi^2}{L^2}$

Notice that E_x and E_z are antisymmetric (and the other components symmetric) with respect to the plane of the gap.

IV. Longitudinal Energy Kick

Instead of plotting the fields at each point in the vicinity of the gap (a most formidable task indeed, in view of the double infinite sums involved in the formulae for the various components), it is preferable to calculate some "integrated" effects of the fields on the particle trajectories. We start with the energy gain per turn associated with the azimuthal component of the electric field. We shall assume that the radio-frequency is the mth harmonic of the angular velocity of the particle, and write

$$\varphi = \varphi_0 + \Omega t = \varphi_0 + \frac{\omega}{m} t$$

The azimuthal component is of the form $E_\varphi = \sum_\nu A_\nu(r,z) \cos\nu\varphi \cos\omega t$

This gives an energy kick of the form

$$\Delta\mathcal{E} = q\int \bar{E}\cdot\bar{ds} = \int_0^{2\pi} r A_m \cos m\varphi \cos(m\varphi - m\varphi_0)\, d\varphi = r A_m \pi \cos m\varphi_0$$

Introducing the actual value of A_m, taken from (5), one finds:

$$\frac{\Delta\mathcal{E}}{qV\cos m\varphi_0} = \sum_{p=1}^{\infty} \frac{m^2}{\mu_{mp}^2} R_m(\mu_{mp} r) \frac{\sinh\gamma_{mp} z + \sinh\gamma_{mp}(L-z)}{\sinh\gamma_{mp} L} \cdot \frac{\int_b^a \frac{R_m}{r}\, dr}{\int_b^a R_m^2\, r\, dr}$$

$$+ \frac{r}{\nu_{mp}^2} \cdot \frac{dS_m(\nu_{mp} r)}{dr} \left[\frac{\nu_{mp}^2}{\tau_{mp}^2} - \frac{k^2\left[\sinh\tau_{mp} z + \sinh\tau_{mp}(L-z)\right]}{\tau_{mp}^2 \sinh\tau_{mp} L} \right] \cdot \frac{S_m(\nu_{mp} a) - S_m(\nu_{mp} b)}{\int_b^a S_m^2\, r\, dr} \qquad (8)$$

The quantity $\frac{\Delta \mathcal{E}}{qV\cos m\varphi_0}$, i.e. the transit time factor, is the loss of energy due to transit time effects through the region occupied by the fields. It is plotted in Figures 3 to 6 for a few representative values of the parameters. Parameters of interest are:

(a) The velocity of the particle, as measured by $\beta = \frac{v}{c}$, and which determines Ω and ω. Our plots refer to a value of β constant throughout the cross-section. This means that the radio frequency must be proportional to $\frac{1}{r}$ at the various points to maintain constant velocity ωr.

(b) The geometric dimensions of the vacuum chamber, as measured by the relative curvature $\rho = \frac{a-b}{(a+b)/2}$ and the aspect ratio $\delta = \frac{a-b}{L}$ of the cross-section.

It is, of course, too much labor to cover the whole range of parameters. We have, consequently, restricted ourselves to those values which show relevant trends. One can, for instance, expect the transit time effects 1) to increase with frequency (i.e. with harmonic number m) 2) to increase with penetration of the fields in the vacuum chamber (which will be particularly large, caeteris paribus, for a square cross-section) and 3) to decrease as the particle accelerates. Figure 3 refers to a set of parameters for which all these effects are important, and makes it clear that higher speeds mean a better transit time-factor. Figure 4 shows that the transit time factor improves when the harmonic number m decreases, and Figure 5 confirms that it also improves with a more

elongated cross-section. We have also computed the energy kick for an accelerator of relative curvature $\rho = 1/6$, but the transit time factor for the range of parameters used in Figures 3 to 5 is practically one (with a maximum excursion of 2.5% from that value), and has not been plotted. Figure 6 gives an idea of the influence of velocity on the transit time factor.

The effect of curvature is apparent in the lack of symmetry of the curves of constant $\Delta\mathcal{E}$ with respect to the center of the cross-section, and is evidenced by a general shift toward the center of curvature. In the linear accelerator of Figure 2, the energy kick from gap to gap would be, for a particle following a trajectory

$$y = v(t - t_0) \qquad \left(\text{with } t_0 = \frac{\varphi_0}{\omega}\right)$$

and where y is counted from the gap:

$$\frac{\Delta\mathcal{E}}{qV\cos\varphi_0} = -\frac{16}{\pi^2}\sum_{1,3}\sum_{1,3}\frac{(-1)^{\frac{m+n}{2}}}{mn}\cdot\frac{\cos m\pi\frac{x}{d}\cos n\pi\frac{z}{L}\left(\gamma_{mn}d\right)^2}{s_{mn}^2 + \left(kd/\beta\right)^2}\left\{1 + \frac{kd\sin\frac{kD}{2\beta}}{\beta s_{mn}\cosh s_{mn}\frac{D}{2d}}\right\}$$

A comparison with the transit time factors of the circular accelerator is given in Figures 3 and 4, where the distance D between gaps in the linear accelerator was taken to be the length of the average circle of the corresponding circular accelerator. More precisely, we took D to be $2\pi\rho d = 2\pi\rho(a-b)$. The resulting graphs show that the worst transit time factors are almost the same in the two cases considered, but that the effect of curvature has been to shift their location toward the axis.

V. Lateral Electric Forces

The radial and Z components of the electric field, as given in equation 5, add up to a term of the form

$$\sum \overline{E}_\nu (r,z) \sin \nu\varphi \cos \omega t$$

A particle travelling on a circle, its azimuth given by $\varphi = \varphi_0 + \frac{\omega}{m} t$, will be subjected to a lateral electric force

$$q \sum \overline{E}_\nu \sin\left(\nu \varphi_0 + \frac{\nu}{m}\omega t\right) \cos \omega t = \frac{q}{2} \sum \overline{E}_\nu \sin\left[\nu\varphi_0 + \left(\frac{\nu}{m}+1\right)\omega t\right]$$
$$+ \frac{q}{2} \sum \overline{E}_\nu \sin\left[\nu\varphi_0 + \left(\frac{\nu}{m}-1\right)\omega t\right] \tag{10}$$

The various terms of this force are oscillatory in nature, and their angular frequencies are given by $\left(\frac{\nu}{m} \pm 1\right)\omega$. One of these frequencies could very well coincide with a betatron frequency. Also, notice that a time-independent force arises from the term $\nu = m$. For these and other reasons, a knowledge of $\overline{E}_\nu$ (r,z) would be highly desirable for a whole range of geometric parameters and values of ν. Explicit formulae for $\overline{E}_\nu$ can easily be deduced from equations (5), and will not be reproduced here. The corresponding quantities for the straight tube can be calculated in a similar fashion. The transverse electric field in that tube is of the form

$$\overline{E}_t = \sum_m \sum_n \overline{f}_{mn}(x,z) \sinh s_{mn} \frac{\pi y}{d} \cos \omega t$$

With the help of the expansion

$$\sinh\left(S_{mn}\frac{\pi y}{d}\right) = -\sum_p \frac{8p\cos p\pi}{\pi\left(4p^2+S_{mn}^2\frac{D^2}{d^2}\right)}\sinh\left(S_{mn}\frac{\pi D}{2d}\right)\sin\frac{2p\pi y}{D}$$

this formula can be rewritten as

$$\bar{E}_x = \sum_{\nu=1}^{\infty}\bar{\mathcal{E}}_\nu \sin 2\pi\frac{\nu y}{D}\cos\omega t$$

where

$$\bar{\mathcal{E}}_\nu = -\frac{64\nu V}{\pi^2 d}\sum_{1,3}\sum_{1,3}\frac{(-1)^{\frac{m+n}{2}}}{n}\sin m\pi\frac{x}{d}\cos n\pi\frac{z}{L}\,\frac{\cos\nu\pi}{4\nu^2+S_{mn}^2\frac{D^2}{d^2}}\,\bar{u}_x$$

$$-\frac{64\nu V}{\pi^2 L}\sum_{1,3}\sum_{1,3}\frac{(-1)^{\frac{m+n}{2}}}{m}\cos m\pi\frac{x}{d}\sin n\pi\frac{z}{L}\,\frac{\cos\nu\pi}{4\nu^2+S_{mn}^2\frac{D^2}{d^2}}\,\bar{u}_y \qquad (11)$$

Let us now change variables, and write

$$Y = v(t-t_0) = y + \frac{D}{2} \qquad \text{with } t_0 = -\frac{m\varphi_0}{\omega} \qquad (12)$$

With this notation, and a radio frequency $\omega = m\frac{v}{D}2\pi$ equal to the mth harmonic, the lateral electric force becomes

$$q\sum\bar{\mathcal{E}}_\nu \sin\nu\frac{2\pi y}{D}\cos\omega t = q\sum\bar{\mathcal{E}}_\nu \sin\left[\frac{\nu}{m}\omega t + \nu\varphi_0 - \nu\pi\right]\cos\omega t$$

Here again the force has components of frequency $\omega\left(\frac{\nu}{m}\pm 1\right)$. It can indeed be put in the form

$$\frac{q}{2}\sum\bar{E}_\nu \sin\left[\nu\varphi_0 + \left(\frac{\nu}{m}+1\right)\omega t\right] + \frac{q}{2}\sum\bar{E}_\nu \sin\left[\nu\varphi_0 + \left(\frac{\nu}{m}-1\right)\omega t\right] \qquad (13)$$

where $\bar{E}_\nu = \frac{\bar{\mathcal{E}}_\nu}{\cos\nu\pi}$. The comparison between lateral electric forces in circular and linear accelerators evidently reduces to a comparison

between the two $\overline{E}_\nu$ appearing in (10) and (13). Differences should result from curvature effects. Figures 7 to 10 show some data on the radial component of $\overline{E}_\nu$. The differences between the curves for the circular and linear accelerators are quite noticeable for square cross-sections and strong curvatures, but have become almost negligible by the time the curvature has decreased to $\rho = 1/6$, as can be inferred by looking at the field in the equatorial plane. The radial electric field along a perpendicular to that plane at the center of the cross section is zero for the linear accelerator. It does <u>not</u> vanish for the circular configuration, and its magnitude, compared to the magnitude along the equatorial plane, gives another estimate of the curvature effect. Some data on the Z component of the electric field, which vanishes along the equatorial plane, are presented in Figure 11. Notice that the curvature has less influence on the vertical fields than on the horizontal fields.

VI. Lateral Magnetic Forces

The meridian components of the magnetic field in the circular accelerator add up, from equation 6, to a vector of the form

$$\sum \bar{H}_\nu \cos\nu\varphi \sin\omega t$$

A particle travelling on a circle, and with azimuth given by $\varphi=\varphi_0+\frac{\omega}{m}t$ (i.e. with a linear velocity $\frac{\omega}{m}r$), will be subjected to a lateral magnetic force

$$\frac{q\nu\mu_0}{2}\sum(\bar{u}_\varphi\times\bar{H}_\nu)\sin\left[\nu\varphi_0+\left(\frac{\nu}{m}+1\right)\omega t\right]-\frac{q\nu\mu_0}{2}\sum(\bar{u}_\varphi\times\bar{H}_\nu)\sin\left[\nu\varphi_0+\left(\frac{\nu}{m}-1\right)\omega t\right] \tag{14}$$

It is desirable, in order to calculate this force, to have plots of $\bar{H}_\nu$ or, more conveniently, of $\nu\mu_0\bar{u}_\varphi\times\bar{H}_\nu=-\nu\mu_0 H_{\nu r}\bar{u}_z+\nu\mu_0 H_{\nu z}\bar{u}_r$. In a similar manner, the transverse magnetic field in the straight tube is of the form

$$\sum_m\sum_n \bar{g}_{mn}(x,z)\cosh S_{mn}\frac{\pi y}{d}\sin\omega t$$

Using the expansion

$$\cosh\left(S_{mn}\frac{\pi y}{d}\right)=\sum_{p=0}^{\infty}\frac{4\cos p\pi D}{\varepsilon_p\,\pi d}\cdot\frac{S_{mn}}{4p^2+S_{mn}^2\frac{D^2}{d^2}}\cdot\sinh\left(S_{mn}\frac{\pi D}{2d}\right)\cos p\frac{2\pi y}{D}$$

where $\varepsilon_p=0$ for $p=0$, $\varepsilon_p=1$ for $p=1,2,\ldots$, we obtain the magnetic field in the form

$$\sum_{\nu=0}^{\infty}\bar{h}_\nu\cos 2\pi\frac{\nu y}{D}\sin\omega t$$

where

$$\bar{h}_\nu = -\frac{32\,\varepsilon_0 V \omega D}{\pi^2 L}\sum_{1,3}\sum_{1,3}\frac{(-1)^{\frac{m+n}{2}}}{m}\cos m\pi\frac{x}{d}\sin n\pi\frac{z}{L}\,\frac{\cos\nu\pi}{\varepsilon_\nu\left[4\nu^2+S^2_{mn}\frac{D^2}{d^2}\right]}\bar{u}_x$$

$$+\frac{32\,\varepsilon_0 V\omega}{\pi^2}\sum_{1,3}\sum_{1,3}\frac{(-1)^{\frac{m+n}{2}}}{n}\sin m\pi\frac{x}{d}\cos n\pi\frac{z}{L}\cdot\frac{\cos\nu\pi}{\varepsilon_\nu\left[4\nu^2+S^2_{mn}\frac{D^2}{d^2}\right]}\bar{u}_z \tag{15}$$

For a particle whose motion is governed by equation (12), the magnetic force is given by

$$\frac{q v\mu_0}{2}\sum(\bar{u}_y\times\bar{H}_\nu)\sin\left[\nu\varphi_0+\left(\frac{\nu}{m}+1\right)\omega t\right]-\frac{q v\mu_0}{2}\sum(\bar{u}_y\times\bar{H}_\nu)\sin\left[\nu\varphi_0+\left(\frac{\nu}{m}-1\right)\omega t\right]$$

where $\bar{H}_\nu = \frac{\bar{h}_\nu}{\cos\nu\pi}$. It is desirable, to calculate this force, to have plots of

$$v\mu_0(\bar{u}_y\times\bar{H}_\nu) = -v\mu_0 H_{\nu x}\bar{u}_z + v\mu_0 H_{\nu z}\bar{u}_x$$

Figures 12 to 14 display these components for a few typical parameters. They afford a comparison with the corresponding values for the circular accelerator. We shall call the vector $v\mu_0(\bar{u}_y\times\bar{H}_\nu)$, which has the dimension volt/meter, the "equivalent electric field" $\bar{E}^m_\nu$. Figures 12 and 13 display the horizontal component of this field along the <u>horizontal</u> axis, and show the importance of curvature effects. This component vanishes along a <u>vertical</u> axis through the center for the linear accelerator, but not for the circular accelerator. The values shown in Figure 14 will consequently provide another measure of the influence of curvature.

The various graphs which have been displayed cover a rather restricted range of parameter values. They will, however, allow a few qualitative conclusions which are quite valuable. Taking the most unfavorable cross-section, namely the square, and assuming a velocity of the order of the velocity of light, we find that, for $\rho = 2/3$ for example, the curvature effects are of the order of a few percent for $\nu = 1$, but become quite important for $\nu = 2$. For a relative curvature of $\rho = 1/6$, we can go up to $\nu = 4$ before curvature effects become noticeable. Generalizing, we advance the opinion that, for the conditions mentioned above, curvature effects become noticeable for azimuthal numbers ν of the order of the ratio $\frac{\text{average radius R}}{\text{side of square d}}$. i.e. for fields having an azimuthal wavelength $\frac{2\pi R}{\nu}$ of the order of $2\pi d$ $(\lambda\!\!\!^{-}_{\varphi} \approx d)$. For flatter cross-sections the effects are reduced.

Acknowledgment

The various summations appearing in this report have been very ably programmed by Dr. J. McNall.

APPENDIX

A derivation of equations (5) and (6) can be outlined as follows. The accelerating structure of Figure 1 (also appearing in Figure 15) is really a flat coaxial line. The fields in a waveguide of any cross-section, excited through a hole in the cylindrical boundary surface, can be expressed as[4]

See Fig. 15

$$\bar{E} = A_0(\zeta)\,\mathrm{grad}\,\phi_0 + \sum_m\sum_p C_{mp}(\zeta)\,\phi_{mp}\,\bar{u}_\zeta + \sum_m\sum_p A_{mp}(\zeta)\,\mathrm{grad}\,\phi_{mp} + \sum_m\sum_p B_{mp}(\zeta)\,\bar{u}_\zeta \times \mathrm{grad}\,\psi_{mp} \quad (16)$$

$$\bar{H} = \alpha_0(\zeta)\,\bar{u}_\zeta \times \mathrm{grad}\,\phi_0 + \sum_m\sum_p \gamma_{mp}(\zeta)\,\psi_{mp}\,\bar{u}_\zeta + \sum_m\sum_p \alpha_{mp}(\zeta)\,\bar{u}_\zeta \times \mathrm{grad}\,\phi_{mp} + \sum_m\sum_p \beta_{mp}(\zeta)\,\mathrm{grad}\,\psi_{mp} \quad (17)$$

where the ϕ's and the ψ's are the eigenfunctions of the two-dimensional Laplacian in the cross-sectional plane, corresponding to Dirichlet and Neumann boundary conditions on the limiting contour (i.e. $\phi = 0$, $\frac{\partial\psi}{\partial n} = 0$ on C_1 and C_2). ϕ_0, in particular, exists in doubly (or multiply) bounded cross-sections only, and is the electrostatic potential obtained by applying a constant potential difference

---

[4] J. Van Bladel "Normal Modes Methods for Boundary-Excited Wave Guides" Zeit. Angew. Math Phys. IX a), pp. 193-202, 1958

between the two boundary curves. For a coaxial line, the eigenfunctions are,

$$\phi_0 = \ln r$$

$$\phi_{mp} = R_m(\mu_{mp} r) \begin{Bmatrix} \sin m\varphi \\ \cos m\varphi \end{Bmatrix}$$

$$\psi_{mp} = S_m(\nu_{mp} r) \begin{Bmatrix} \sin m\varphi \\ \cos m\varphi \end{Bmatrix}$$

where the R_m and S_m have been defined in (3) and (4). The still unknown Z-dependent coefficients can be found from the following differential equations, taken from Reference 4,

$$\frac{dA_0}{dz} + j\omega\mu\alpha_0 = \frac{d\alpha_0}{dz} + j\omega\varepsilon a_0 = 0$$

$$\frac{dA_{mp}}{dz} + j\omega\mu\alpha_{mp} - C_{mp} = \frac{d\alpha_{mp}}{dz} + j\omega\varepsilon A_{mp} = \alpha_{mp} + \frac{j\omega\varepsilon}{\mu_{mp}^2} C_{mp} = 0$$

$$\frac{d\beta_{mp}}{dz} - j\omega\varepsilon B_{mp} - \gamma_{mp} = \frac{dB_{mp}}{dz} - j\omega\mu\beta_{mp} = 0$$

$$B_{mp} - \frac{j\omega\mu\gamma_{mp}}{\nu_{mp}^2} = \frac{V}{\nu_{mp}^2 \iint_S \psi_{mp}^2 r\,dr} \begin{Bmatrix} 0 \\ S_m(\nu_{mp} a) - S_m(\nu_{mp} b) \end{Bmatrix}$$

and where we have made use of the fact that $E_z = 0$ and $E_\varphi = \frac{V}{a}\delta(\varphi)$ at r = a, $E_\varphi = \frac{V}{b}\delta(\varphi)$ at r = b along the cylindrical boundary. To solve these differential equations, we still need boundary conditions at Z = 0 and Z = L. For these values of z, the

tangential electric field is imposed: it is $\frac{V}{r}\,\delta(\varphi)\,\bar{u}_\varphi$. If we set Z = 0 and Z = L in (16), and equate the transverse part of the right hand side (i.e. all terms but those of the form $c\phi\,\bar{u}_z$) to $\frac{V}{r}\,\delta(\varphi)\,\bar{u}_\varphi$, we find

$$A_0 = 0$$

$$A_{mp}(0) = A_{mp}(L) = \frac{mV}{\mu_{mp}^2 \iint \phi_{mp}^2\, r\,dr} \begin{Bmatrix} \int_b^a \frac{R_m}{r}\,dr \\ 0 \end{Bmatrix}$$

$$B_{mp}(0) = B_{mp}(L) = \frac{V}{\nu_{mp}^2 \iint \psi_{mp}^2\, r\,dr} \begin{Bmatrix} 0 \\ S_m(\nu_{mp}a) - S_m(\nu_{mp}b) \end{Bmatrix}$$

These relations allow the determination of all Z dependent coefficients in (16) and (17), and lead, after a few trivial analytical steps, to equations (5) and (6) of the text.

LIST OF CAPTIONS

Fig. 1 Circular accelerator with radial gap.

Fig. 2 Linear accelerator with periodic array of gaps.

Fig. 3 Distribution of the transit time factor throughout the cross-section for $\rho = 2/3$ and a square cross-section (i.e. $\sigma = 1$) for (a) the circular accelerator (b) the linear accelerator. The gap is excited on the third harmonic of the angular velocity, and velocities $\frac{1}{3}c$ and $\frac{2}{3}c$ are considered. For a velocity equal to C, the factor is practically equal to one.

Fig. 4 Transit time factor in the same conditions as in Fig. 3, except that the gap is excited on the second harmonic.

Fig. 5 Transit time factor for a circular accelerator in the same conditions as in Fig. 3, except that the cross-section is rectangular with aspect ratio two.

Fig. 6 Transit time factor as a function of velocity for a circular accelerator of square cross-section. The particle is at the center of the cross-section.

Fig. 7 Radial component of $\overline{E}_3$ in the equatorial plane (i.e. along line AB) for a square cross-section and $\rho = 2/3$.

Fig. 8 Radial component of $\overline{E}_3$ along a perpendicular CD to the equatorial plane at the center. Relative curvature $\rho = 2/3$. For $\rho = 1/6$, $\tau = 1$ this component is less than 10^{-3}.

Fig. 9 Radial component of $\overline{E}_1$ in the equatorial plane (i.e. along line AB) for a square cross-section and $\rho = 2/3$, $\beta = 1$. The curves for $\beta = 1/3$ are very close to those for $\beta = 1$, and are not shown explicitly.

Fig. 10 Radial component of $\overline{E}_3$ in the equatorial plane (i.e. along line AB) a) for $\beta = 1/3$ $\rho = 2/3$, and a rectangular cross-section with $\tau = 2$ (curves for $\beta = 1$ are undistinguishable) b) for $\beta = 1/3$, a square cross-section and weak curature ($\rho = 1/6$)

Fig. 11 Vertical component of $\overline{E}_3$ along a perpendicular CD to the equatorial plane for $\beta = 1/3$. For $\rho = 1/6$ and $\tau = 1$, the two curves are undistinguishable.

Fig. 12 Radial component of $\overline{E_3^m}$ along the horizontal axis for a square cross-section, a curvature $\rho = 2/3$, and two values of the velocity.

Fig. 13 Radial component of $\overline{E_3^m}$ along the horizontal axis for a square cross-section, the velocity of light and two different curvatures.

Fig. 14 Radial component of $\overline{E^m}$ along vertical axis through center for $\beta = 1$ and a variety of conditions.

Fig. 15 Short coaxial line.

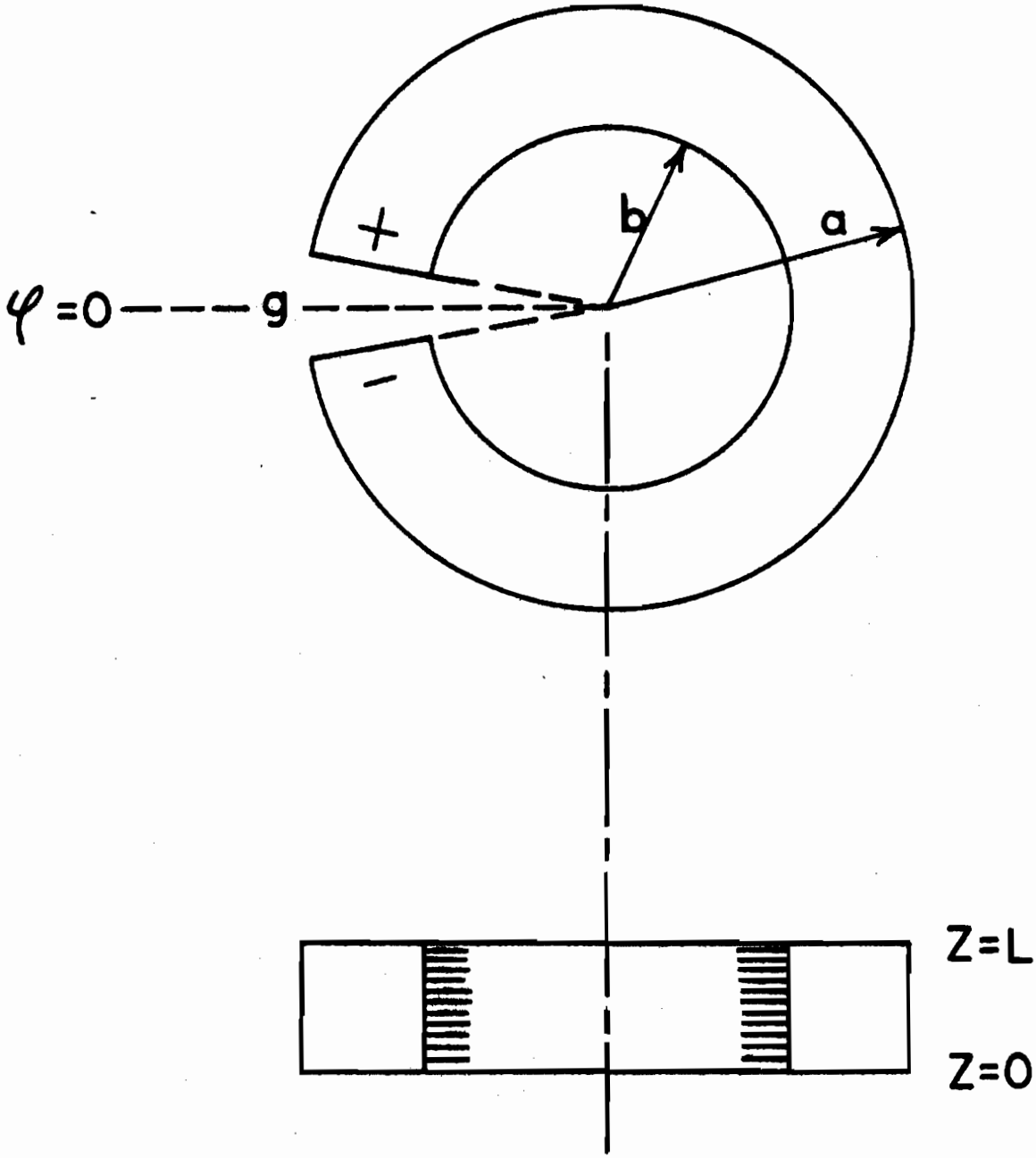

Figure 1

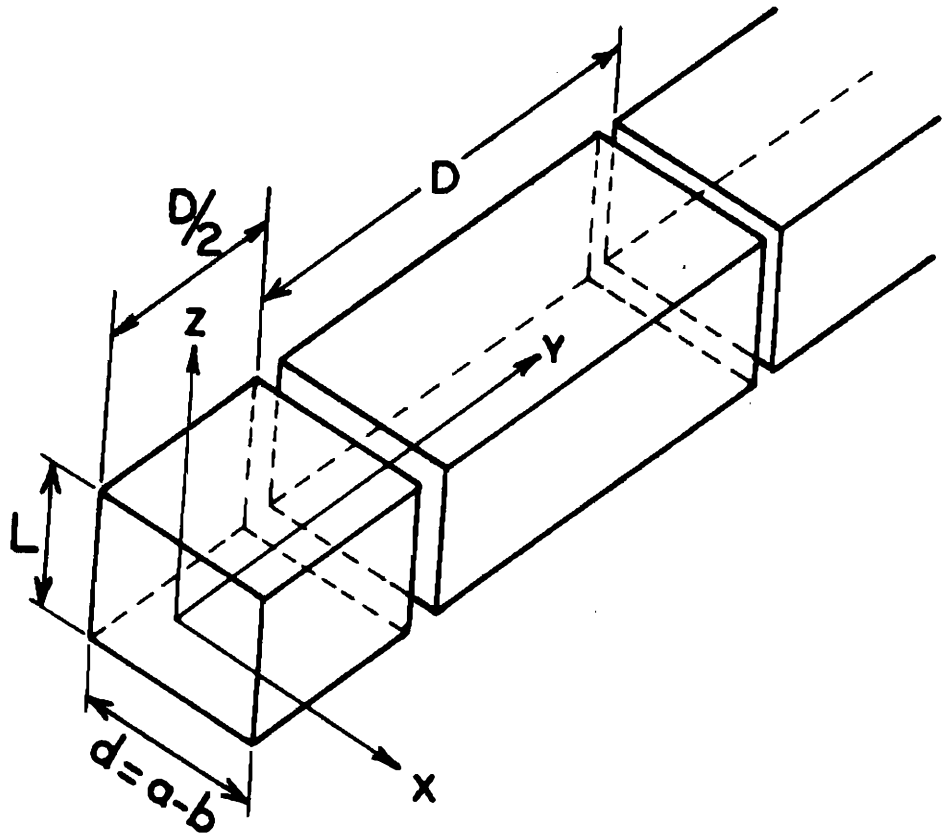

Figure 2

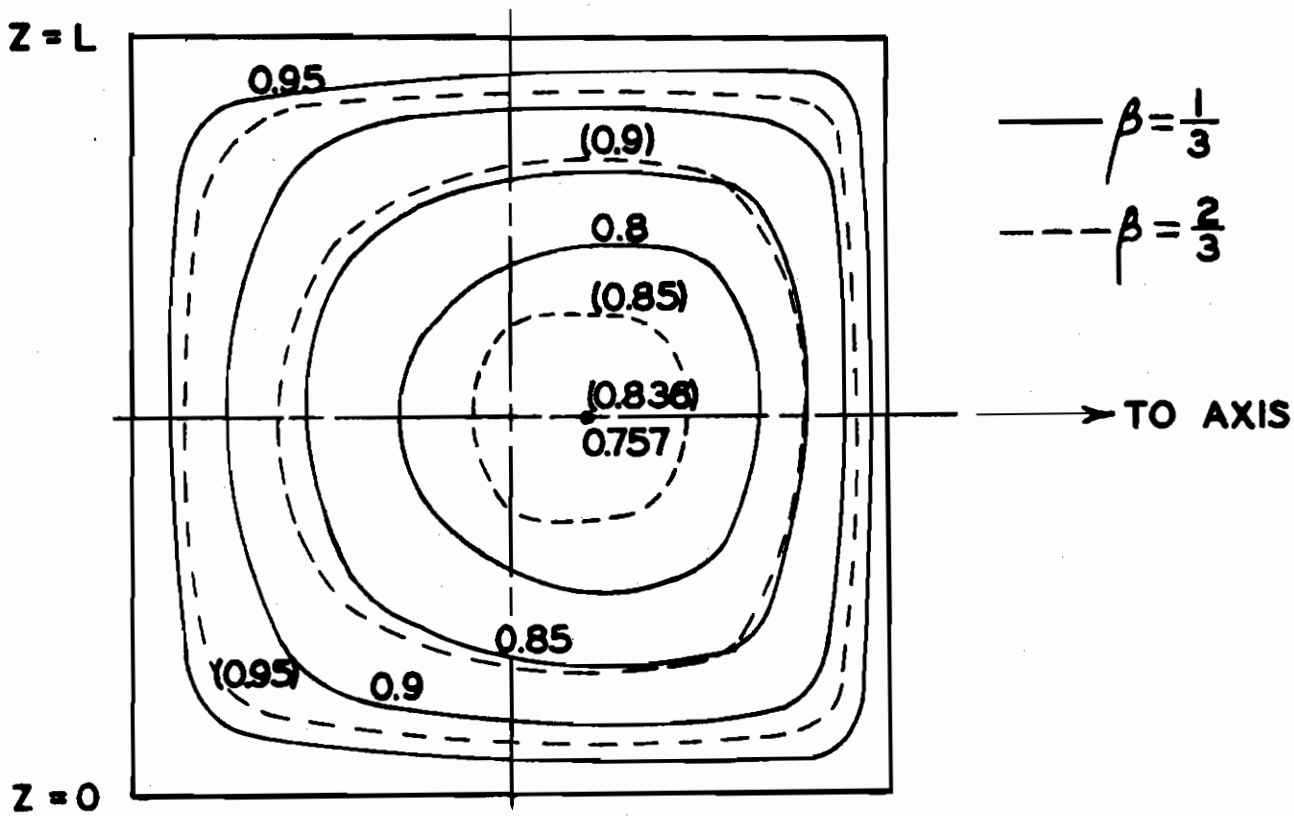
Z = L
0.95
(0.9)
0.8
(0.85)
(0.836)
0.757
0.85
(0.95)
0.9
Z = 0
TO AXIS
$\beta = \frac{1}{3}$
$\beta = \frac{2}{3}$

(a)

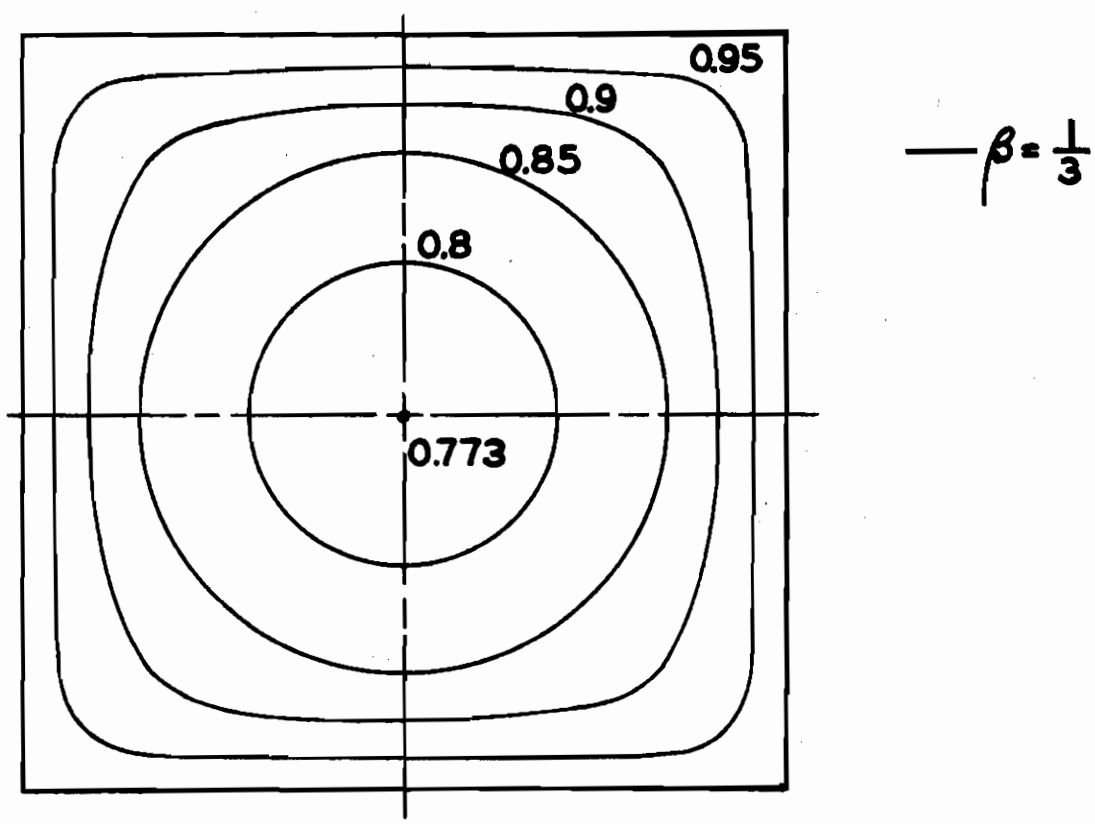
0.95
0.9
0.85
0.8
0.773
$\beta = \frac{1}{3}$

(b)

Figure 3

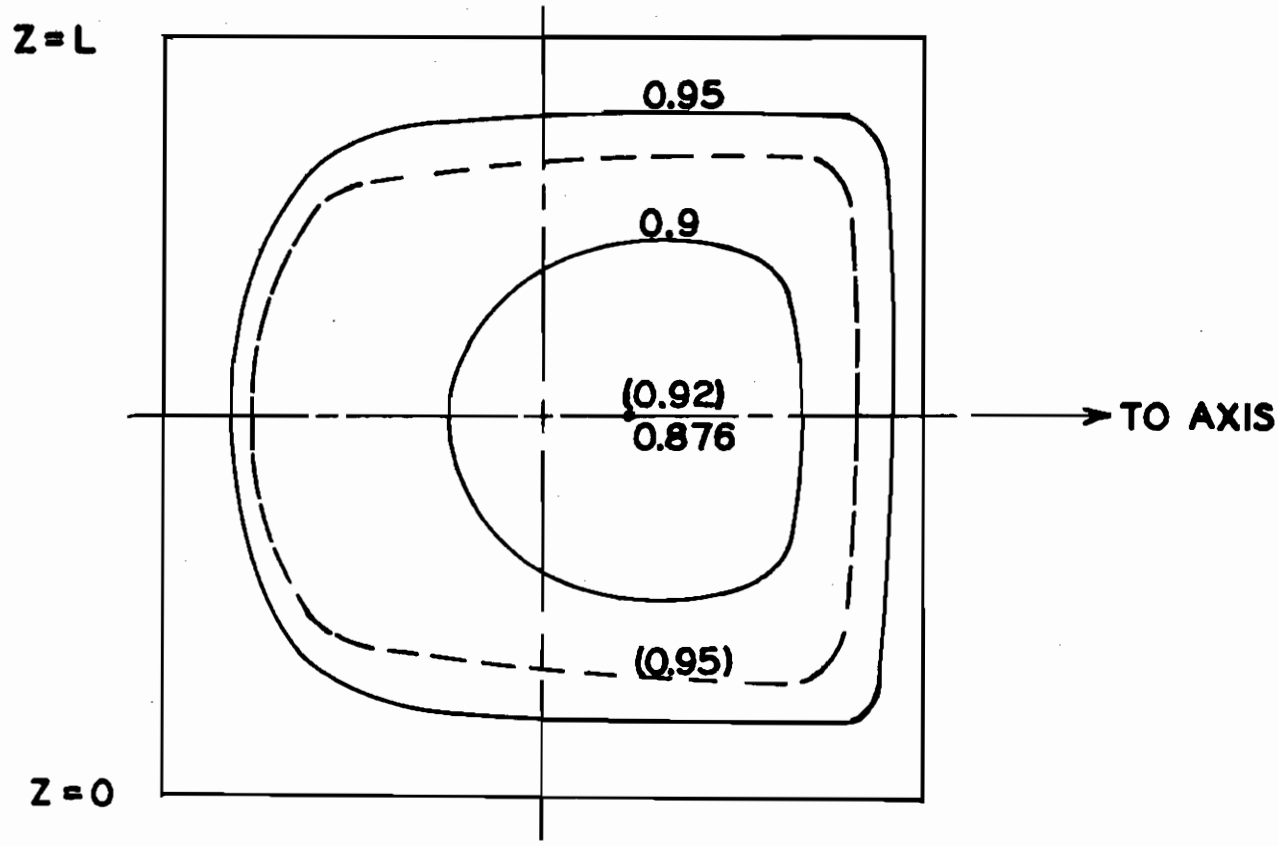

(a)

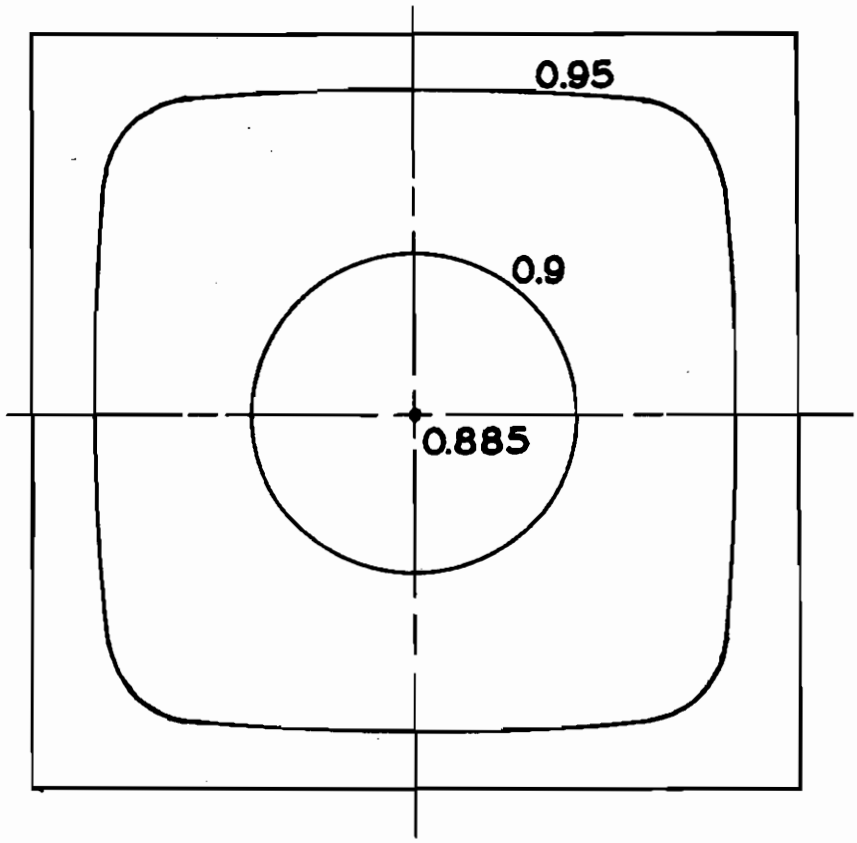

(b)

Figure 4

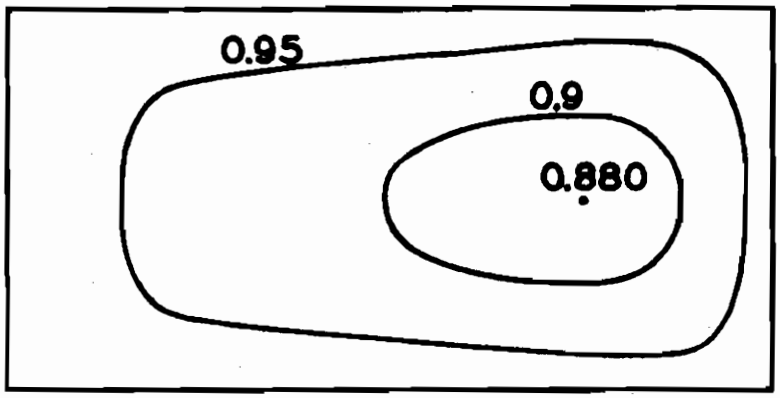

Figure 5

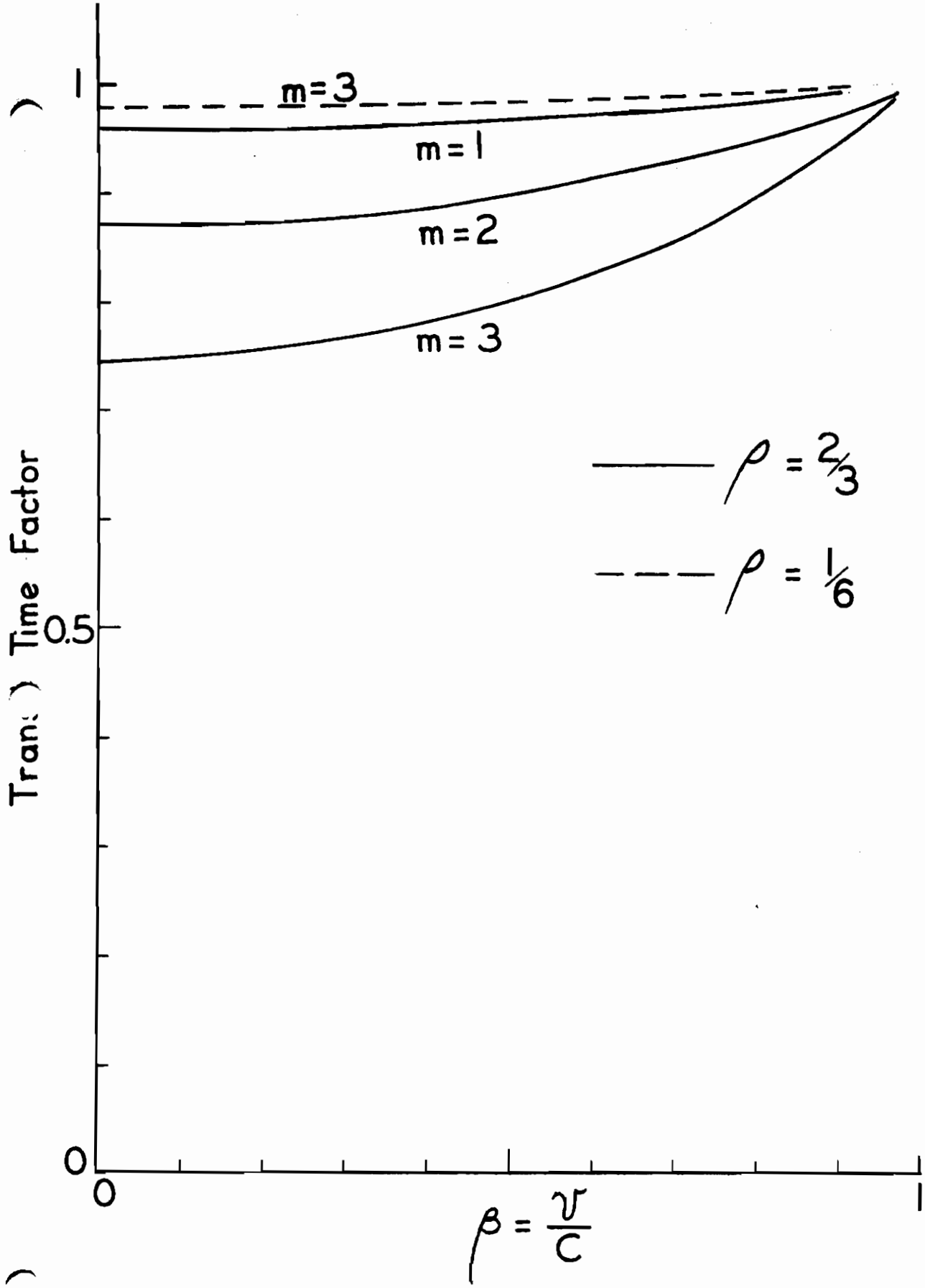

Figure 6

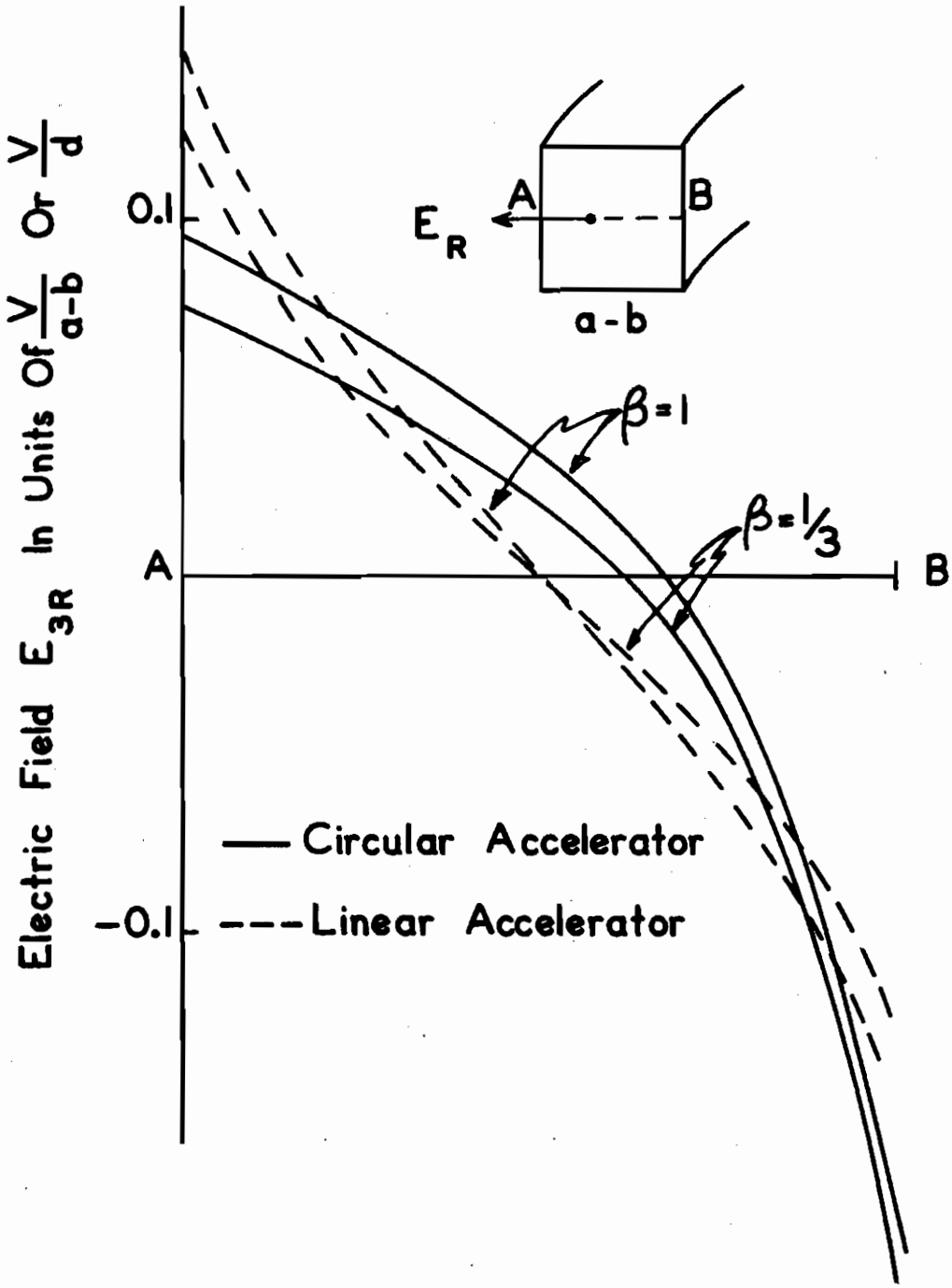
Electric Field E_{3R} In Units Of $\frac{V}{a-b}$ Or $\frac{V}{d}$
0.1
-0.1
A
B
E_R
a - b
$\beta = 1$
$\beta = 1/3$
Circular Accelerator
Linear Accelerator

Figure 7

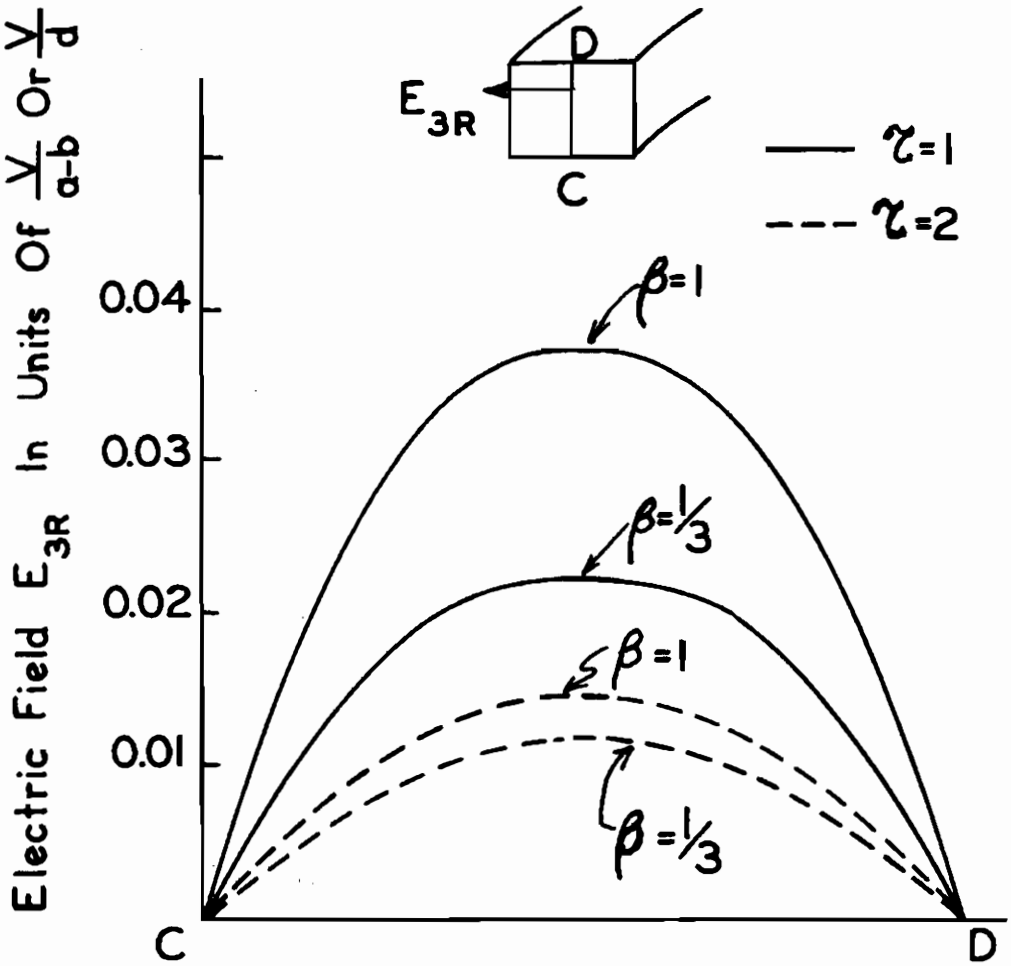
Electric Field E_{3R} In Units Of $\frac{V}{a-b}$ Or $\frac{V}{d}$
0.04
0.03
0.02
0.01
C
D
E_{3R}
D
C
$\tau=1$
$\tau=2$
$\beta=1$
$\beta=1/3$
$\beta=1$
$\beta=1/3$

Figure 8

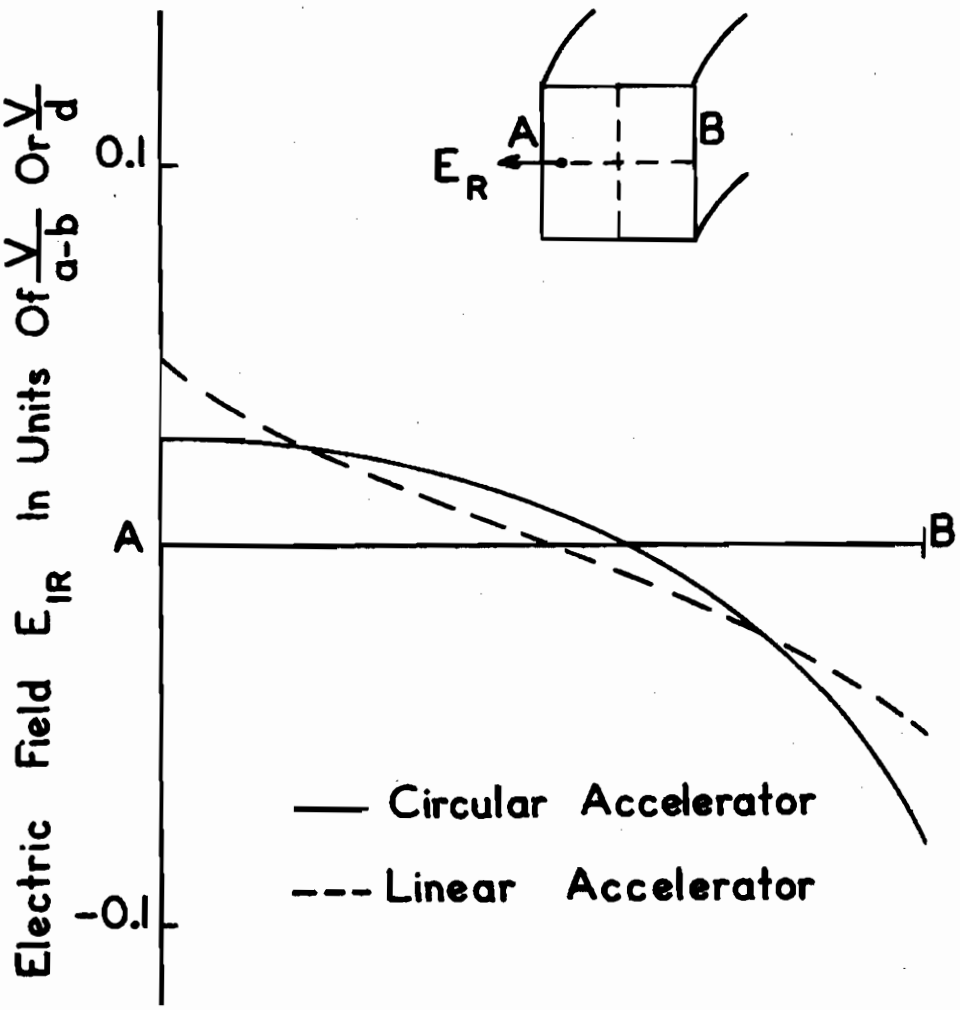
Electric Field E_{IR} In Units Of $\frac{V}{a-b}$ Or $\frac{V}{d}$
0.1
-0.1
A
B
E_R
Circular Accelerator
Linear Accelerator

Figure 9

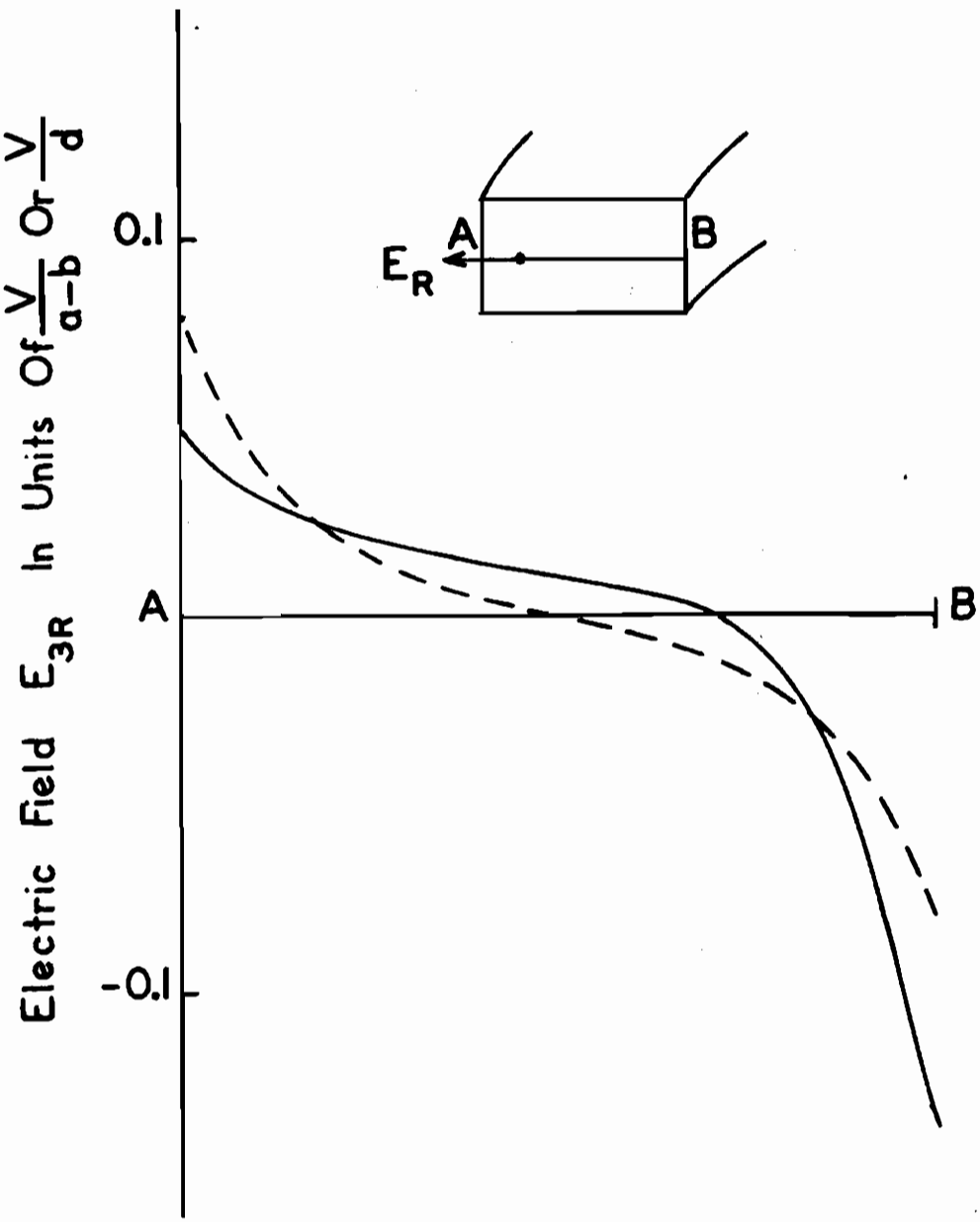
Electric Field E_{3R} In Units Of $\frac{V}{a-b}$ Or $\frac{V}{d}$
0.1
-0.1
A
B
E_R
A
B

Figure 10 a)

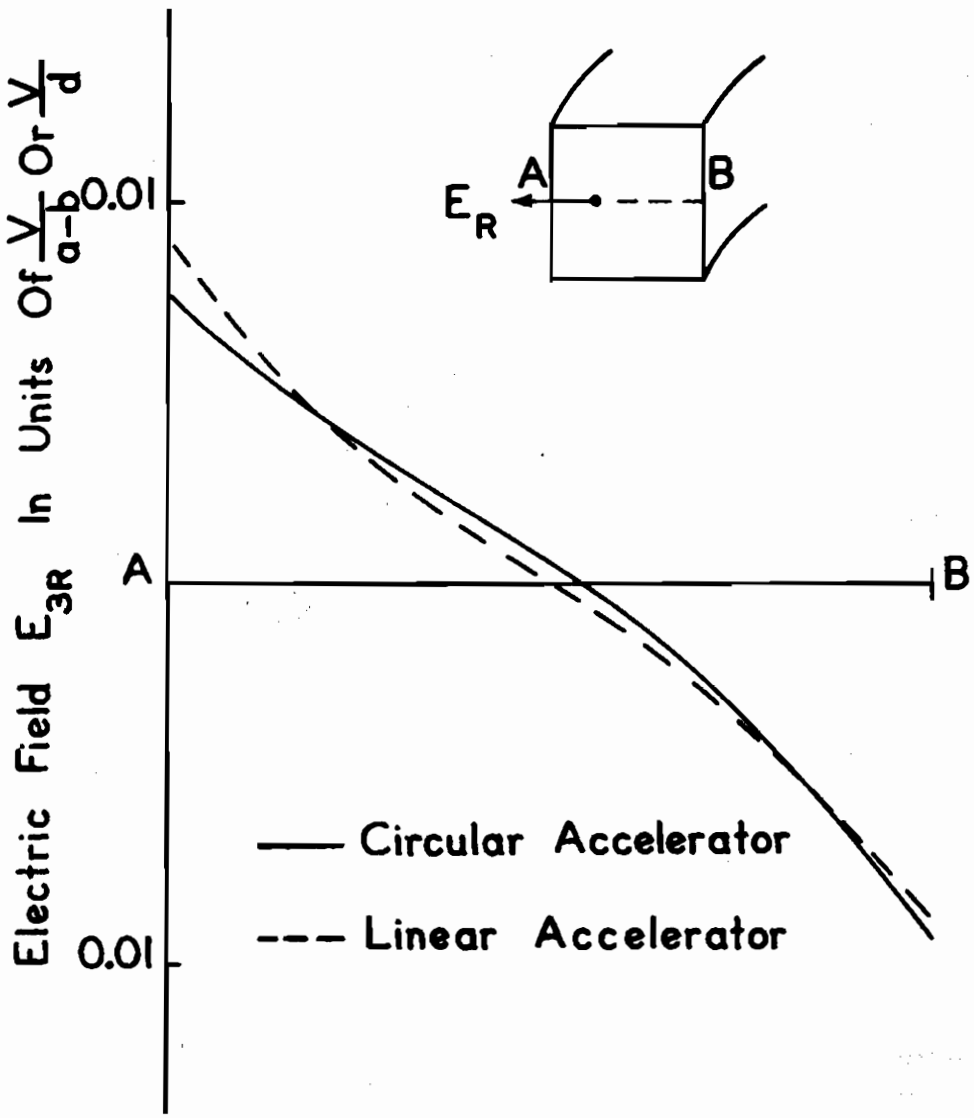
Electric Field E_{3R} In Units Of $\frac{V}{a-b}$ Or $\frac{V}{d}$
0.01
0.01
A
B
E_R
A
B
Circular Accelerator
Linear Accelerator

Figure 10 b,

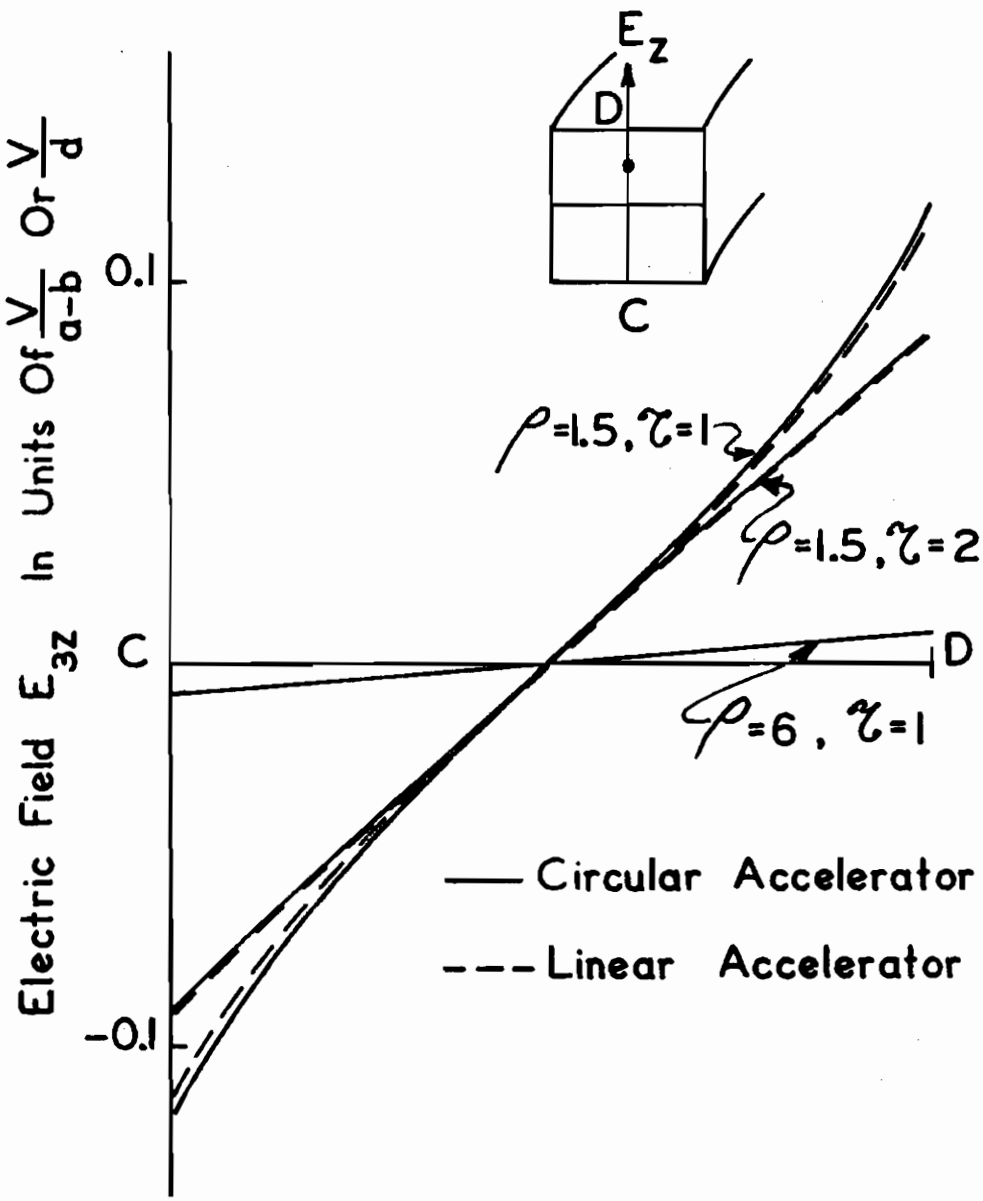
Electric Field E_{3z} In Units Of $\frac{V}{a-b}$ Or $\frac{V}{d}$
0.1
C
-0.1
E_z
D
C
ρ=1.5, τ=1
ρ=1.5, τ=2
D
ρ=6 , τ=1
Circular Accelerator
Linear Accelerator

Figure 11

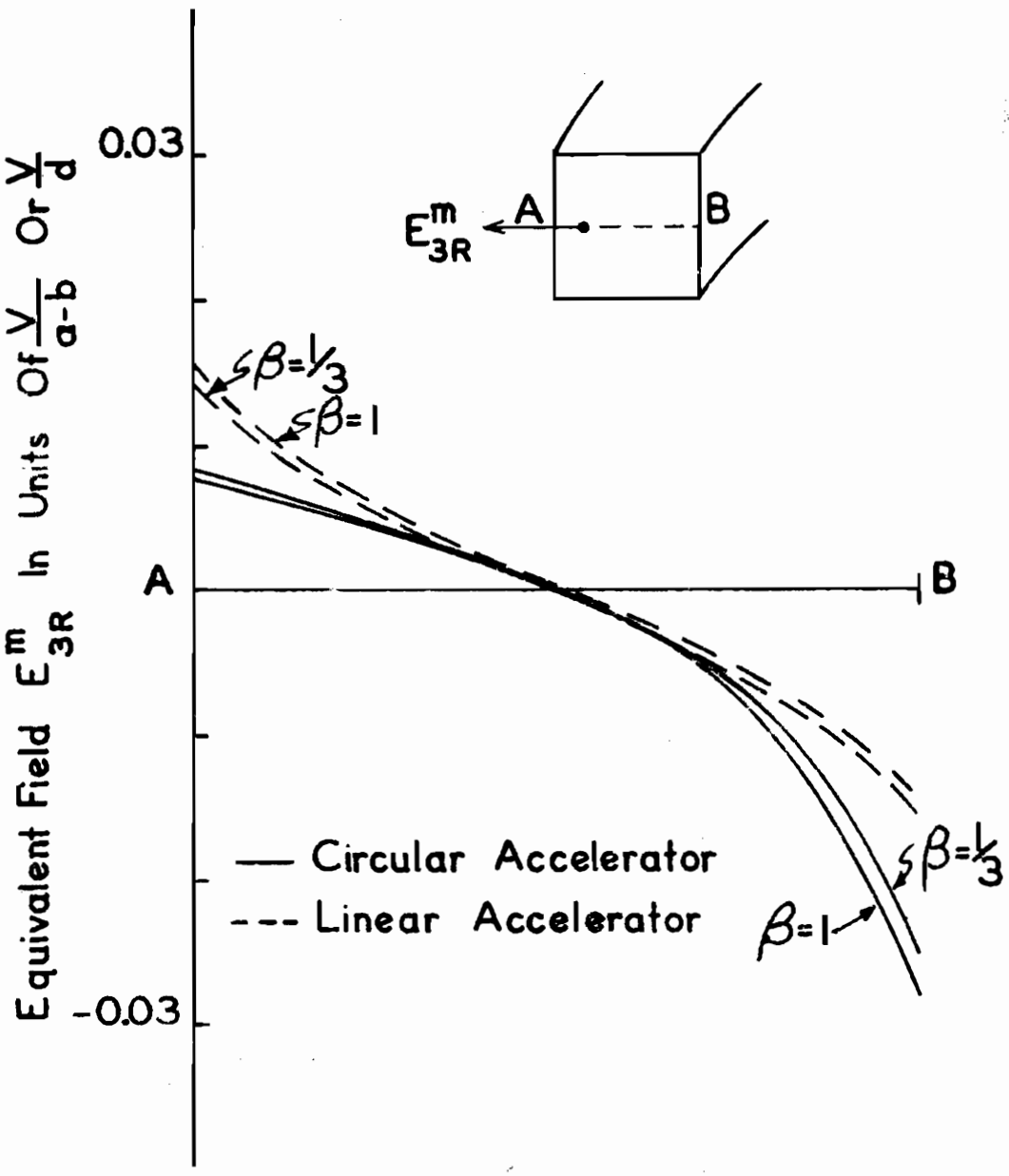
Equivalent Field E^m_{3R} In Units Of $\frac{V}{a-b}$ Or $\frac{V}{d}$
0.03
-0.03
A
B
E^m_{3R}
A
B
$\beta=1/3$
$\beta=1$
$\beta=1/3$
$\beta=1$
— Circular Accelerator
--- Linear Accelerator

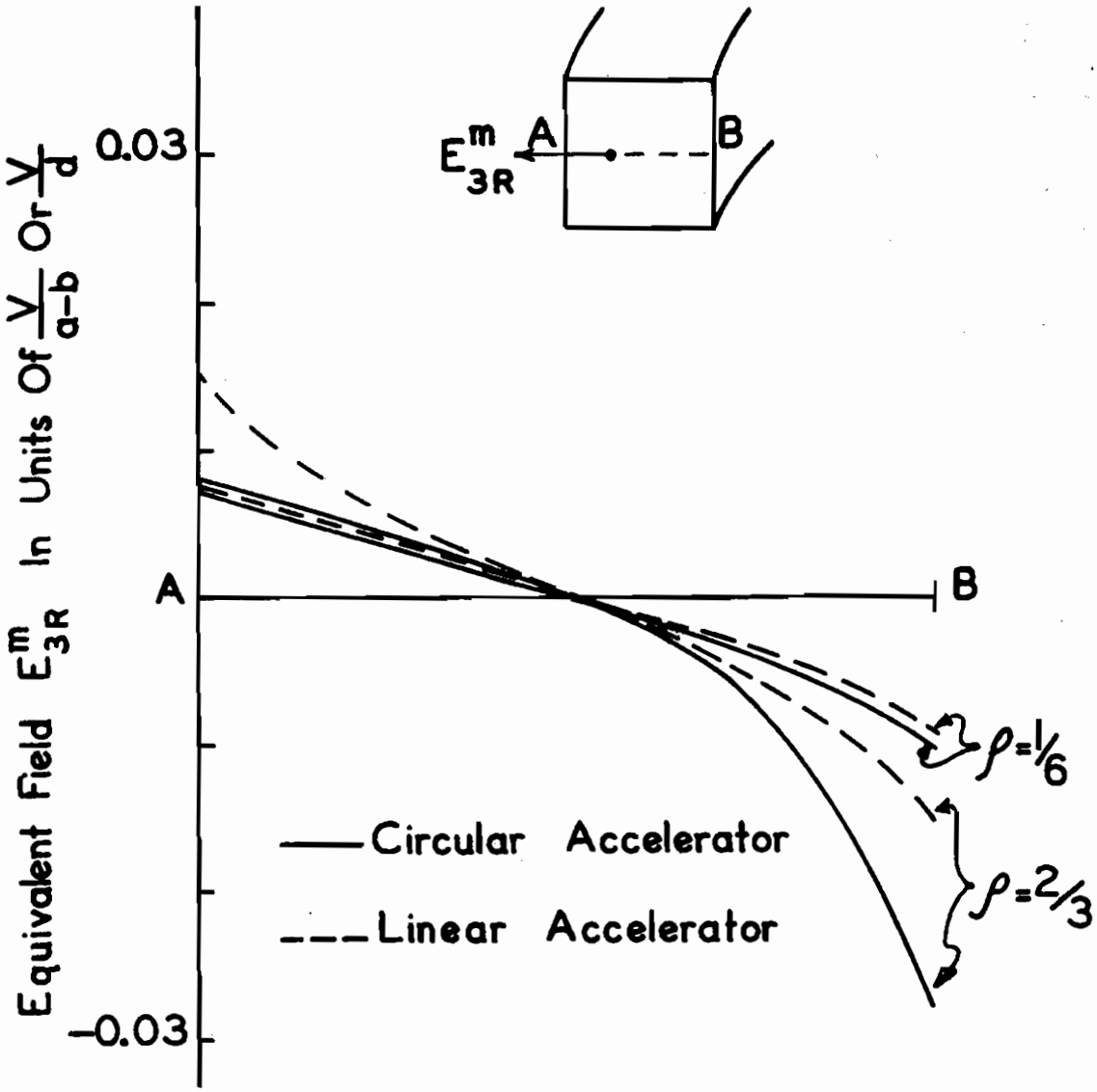
Equivalent Field E^m_{3R} In Units Of $\frac{V}{a-b}$ Or $\frac{V}{d}$
0.03
-0.03
A
B
E^m_{3R}
A
B
$\rho = 1/6$
$\rho = 2/3$
Circular Accelerator
Linear Accelerator

Figure 13

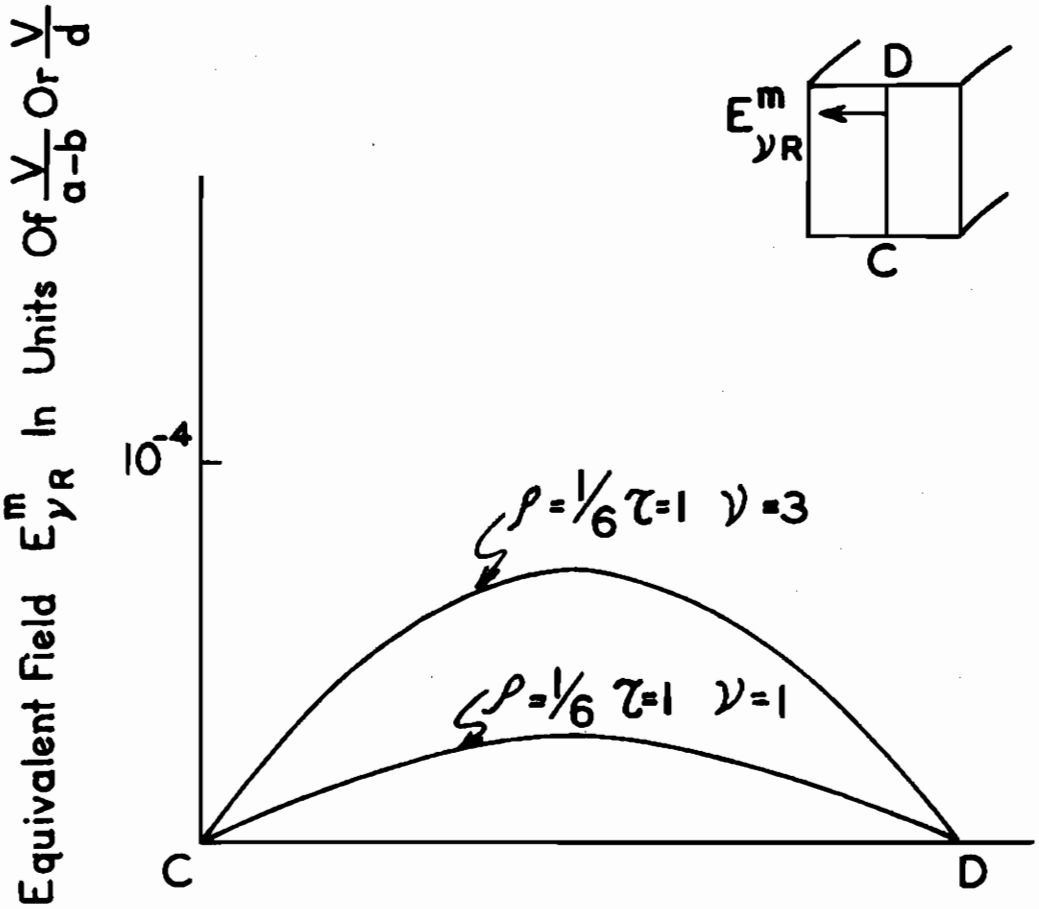
Equivalent Field $E^m_{\nu R}$ In Units Of $\frac{V}{a-b}$ Or $\frac{V}{d}$
10^{-4}
$\rho = 1/6\ \tau = 1\ \nu = 3$
$\rho = 1/6\ \tau = 1\ \nu = 1$
C
D
$E^m_{\nu R}$
D
C

Figure 14a

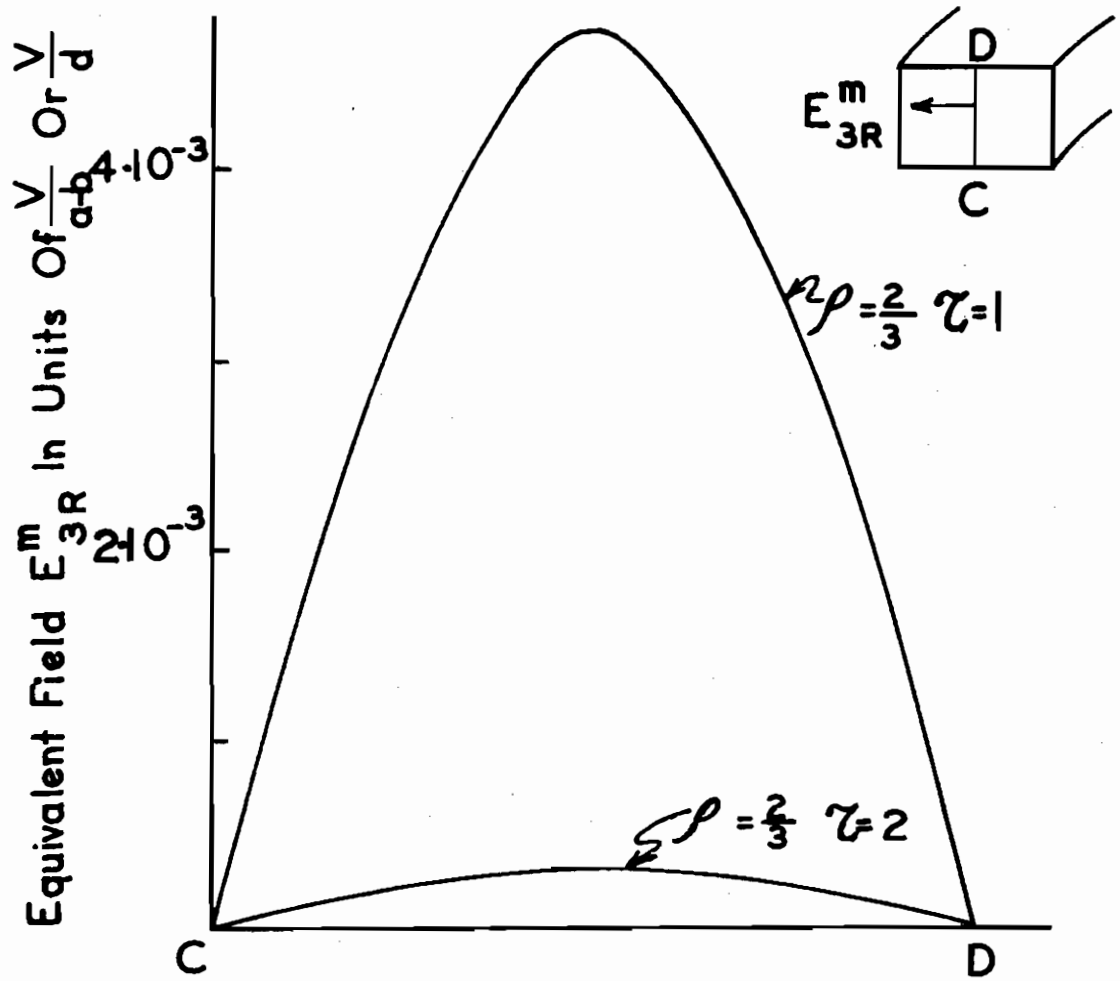
Equivalent Field E^m_{3R} In Units Of $\frac{V}{a-b}$ Or $\frac{V}{d}$
$4 \cdot 10^{-3}$
$2 \cdot 10^{-3}$
C
D
$\rho = \frac{2}{3}$ $\tau = 1$
$\rho = \frac{2}{3}$ $\tau = 2$
E^m_{3R}
D
C

Figure 14 6

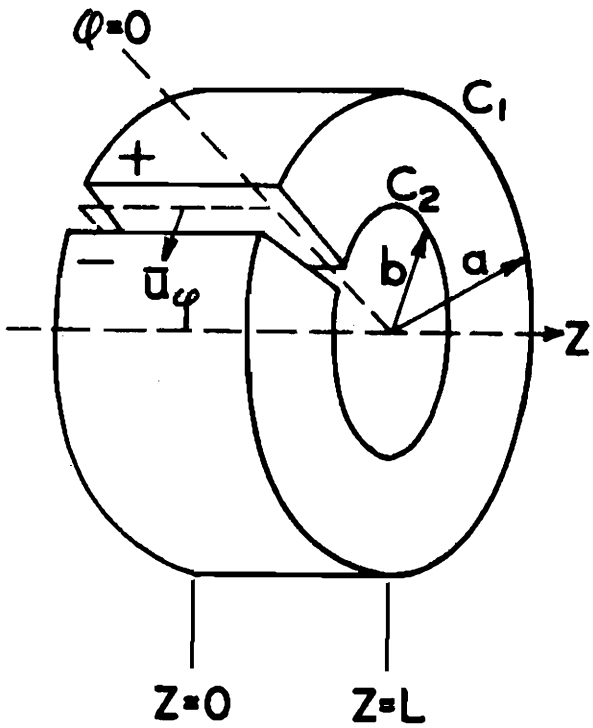

Figure 15